A02-13933

AIAA 2002-0799

Landing Gear Aerodynamic Noise Prediction Using Unstructured Grids

Frederic J. Souliez, Lyle N. Long, Philip J. Morris and Anupam Sharma
The Pennsylvania State University
University Park, PA

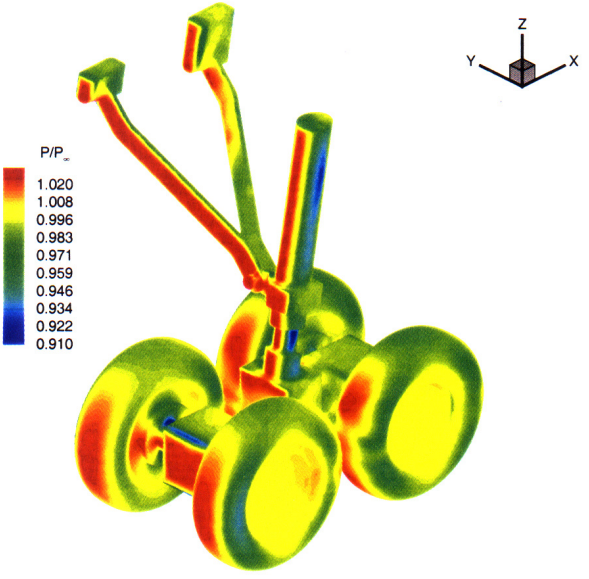

40th AIAA Aerospace Sciences Meeting & Exhibit
14 – 17 January 2002 / Reno, NV

AIAA-2002-0799

LANDING GEAR AERODYNAMIC NOISE PREDICTION USING UNSTRUCTURED GRIDS

Frederic J. Souliez*, Lyle N. Long†, Philip J. Morris‡ and Anupam Sharma†

Department of Aerospace Engineering
The Pennsylvania State University
University Park, PA 16802
lnl@psu.edu

ABSTRACT

Aerodynamic noise from a landing gear in a uniform flow is computed using the Ffowcs Williams-Hawkings (FW-H) equation. The time accurate flow data on the surface is obtained using a finite volume flow solver on an unstructured grid. The FW-H equation is solved using surface integrals over the landing gear surface and over a permeable surface away from the landing gear. Two geometric configurations are tested in order to assess the impact of two lateral struts on the sound level and directivity in the far-field. Predictions from the FW-H code are compared with direct calculations by the flow solver at several observer locations inside the computational domain. The permeable FW-H surface predictions match those of the flow solver in the near-field. Far-field noise calculations coincide for both integration surfaces. The increase in drag observed between the two landing gear configurations is reflected in the sound pressure level and directivity mainly in the streamwise direction.

INTRODUCTION

The Ffowcs Williams-Hawkings (FW-H) equations have recently been used with permeable surfaces in order to predict aerodynamic noise[1,2]. It is an inexpensive method to include the quadrupole source terms inside the FW-H surface without performing any volume integrations. This can significantly improve the accuracy of the noise predictions at locations where nonlinear interactions in the flow cannot be ignored. This is notably the case with highly turbulent flows such as high Reynolds number jet and wakes. It is also only slightly more expensive to use than a moving Kirchhoff surface (see Özyörük and Long[3]), but without the limitations of Kirchhoff methods.

The motivation for predicting the far-field noise generated by a 4-wheel landing gear stems from the increasing contribution of airframe noise to the overall sound level of an aircraft in its landing approach. Early studies in the 1970's by Heller and Dobrzynski[4] showed that high-lift devices such as slats and flaps, as well as deployed gears, generated noise levels 10 dB higher than those of an aircraft in its "clean" cruise configuration. Aerospatiale (now EADS Airbus) investigated the noise produced by several Airbus airplanes, which seems to indicate that noise from high-lift devices is likely to dominate for medium size aircraft, while landing gear noise seems more of a problem for existing and future high capacity aircraft. The importance of investigating landing gear noise is reinforced by Airbus Industry plans to extend the Airbus family towards a high capacity aircraft.

Heller and Dobrzynski carried out a series of tests with both scale models[4] and full scale models[5], which underscored the lack of detailed geometric features with model-scale experiments and their effects on high frequency noise. These early experiments also showed that there is an increase in noise radiation from tandem axle configurations, which is the second test case in the present study. However, it was also found during the full scale experiment that struts, braces and other small features contribute significantly to the overall sound level. A more recent work by Dobrzynski et al[6] where the impact of various gear sizes and configurations is measured, illustrates the difficulty in using scale-model results for full-scale noise predictions. The actual simulation of the landing gear flow field is also of interest since it potentially affects the inflow of flaps located downstream. This was experimentally shown

---

* Graduate Research Assistant
† Professor, Assoc. Fellow, AIAA
‡ Boeing / A.D. Welliver Professor, Fellow, AIAA

by Stoker et al[7] during a wind tunnel investigation of the airframe noise radiated by a model-scale Boeing 777, in which case a second high-frequency noise source from the flap system is only seen in the presence of the landing gear. This landing gear – flap interaction noise source was even shown to increase significantly by using a highly detailed gear geometry.

As already performed in a previous study by the same authors[8], the goal here is to combine the flexibility of unstructured grids with the FW-H equation. We use the Parallel Unstructured Maritime Aerodynamics (PUMA) code for generating the flow data. PUMA has been validated in several instances for simulating time-accurate flow data[9,10]. The aim in the present case is to evaluate the impact on the noise directivity and intensity of two landing gear geometries (LDG1 and LDG2). It is expected to observe larger pressure fluctuations and a more complex three-dimensional flow in the case involving two additional struts (LDG2).

Comparisons with another numerical experiment being carried out at NASA Langley may be available in the near future. A similar run using the CFL3D structured solver with as many as 13.5 million points is under way. A landing gear flow simulation has already been performed by Strelets[11] using a simplified gear and a Detached Eddy Simulation (DES) turbulence model on a 2.5 million point structured mesh.

THE GRIDS

The grids used for the simulation of the flow over both landing gear configurations were generated using Gridgen[12]. Figures 1 and 2 show an overall view of the meshes on the landing gear surfaces with and without lateral struts respectively.

The first mesh consists of about 80,000 surface triangles, for a total of about 880,000 tetrahedra in the volume mesh. The second mesh reused as much of the previous grid features as possible. With two additional struts, the number of triangles on the surface went up to 135,000, with about 1.2 million tetrahedral cells.

Specific attention was given to the cell clustering between the front and rear wheels, in order to capture as much of the wake from the upstream wheel impinging on the downstream wheel. Flow separation from the fore wheel and wake impingement on the aft are expected to generate large unsteady pressure fluctuations and therefore noise. With the second geometry, great care was given to the mesh refinement between the two lateral struts, with the aft strut in the wake of the fore strut. The smallest geometric features were not overly simplified, since they have been shown to generate high frequency noise as explained in a later section describing the Ffowcs Williams – Hawkings equation.

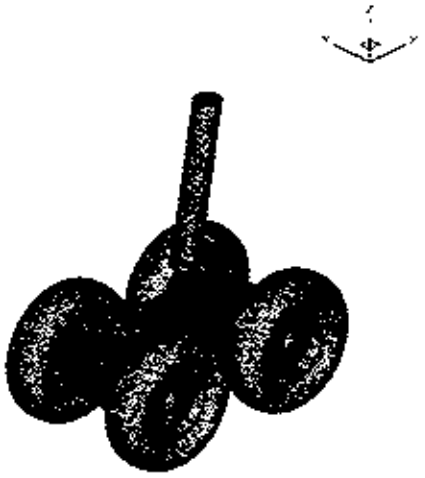

Figure 1- Surface mesh of first landing gear configuration(LDG1)

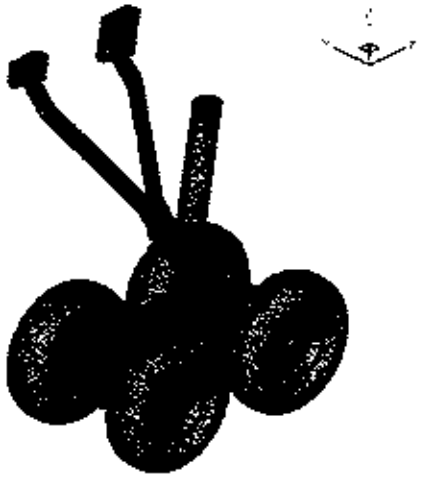

Figure 2 - Surface mesh of second landing gear configuration (LDG2)

As shown in Figure 3 for the second geometry (LDG2), a porous FW-H integration surface was used in addition to the flow data collected on the landing gear surfaces themselves. This will help determine the magnitude of the quadrupole source term for this low Mach number flow. Permeable FW-H surfaces were used for both geometries, with about 13,000 triangles in the first case, and 15,500 triangles in the case including two lateral struts. This coarsening mesh away from the solid surface is due to computer limitations. It should not be able to support the higher frequency pressure

fluctuations. The advantage of these porous surfaces is that they can capture quadrupole-like terms without having to perform any volume integration. FW-H surfaces can be used in regions dominated by nonlinear effects (unlike the Kirchhoff formulations).

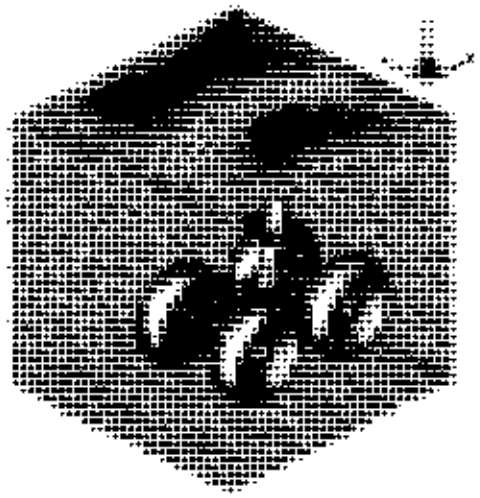

Figure 3- Partial view of the porous FW-H surface around second gear configuration (LDG2)

During the time-accurate runs (all made on parallel Beowulf PC clusters), the FW-H faces would be flagged on each running CPU, so that unsteady flow data would be output at a prescribed sampling rate (slightly below 70 kHz). This is meant to maintain at least 10 data points per wavelength, the shortest wavelength being 40 times that of the simulated shedding frequency (about 147 Hz for the simulated flow conditions and a Strouhal number of 0.2 based on the wheel diameter).

The Gibbs-Poole-Stockmeyer algorithm[13] was used to speed-up the communication process between CPUs. As shown in Figure 4, this procedure divides the domain into slices that minimize the number of messages between each processor, so that each CPU exchanges data with at most two neighboring CPUs. The time step for the unsteady simulations is determined by the smallest cell characteristic length. At a CFL number of 0.95, this yields a time step of 0.86E-08 second for the first grid, and 1.90E-08 second for the second grid (due mostly to some improved CAD work in the original geometry file). The numerical conditions were dictated by the CFL3D run performed at Langley: the Reynolds' number based on the wheel diameter is 1.25 million, for a free stream Mach number of 0.2, a free stream pressure of about 3 atmospheres and a corresponding viscosity of 1.142 Kg/m^3. The actual wheel diameter of the landing gear model is 9.4 cm.

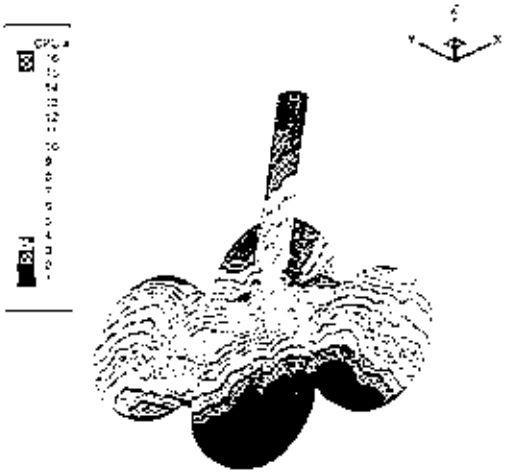

Figure 4- GPS partitioning on the first landing gear surface (LDG1) across 16 processors

FLOW SOLVER

PUMA is the computer program that was used to run the unsteady calculations. It is a finite volume, Runge-Kutta time-marching code that solves the compressible Navier-Stokes equations and uses unstructured grids. It uses the Message Passing Interface (MPI) library for parallel implementation. No RANS or LES model was used. Its scaling performance for the two configurations is illustrated in figure 5.

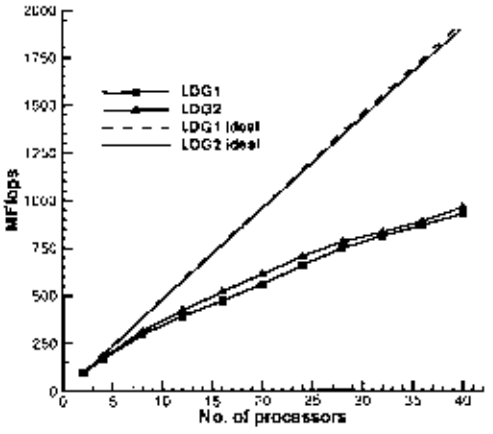

Figure 5- Parallel speed up on COCOA2 for both landing gear configurations

The flop performance is slightly higher for the second case for any given number of CPUs, since the ratio of computation over communication is greater for a larger grid. The facility used to perform the computation is the latest our two Cost effective Computing Arrays (COCOA[14] and COCOA2[15]). COCOA2 is a Beowulf cluster comprised of 20 nodes each having dual 800 MHz Pentium III and 1 GB RAM. The cluster has dual fast-Ethernet on each node and all the nodes are connected using two HP2524 switches with channel bonding for increased data communication. These machines run Redhat Linux (version 7.0) and the gcc compiler.

CFD RESULTS

Simulations were carried out over two cycles based on the expected shedding frequency of the wheel diameter. Each simulation took about 90 days on 24 CPUs. Data were sampled only for the second cycle to minimize the effects of the starting conditions. Local time stepping was initially used to accelerate the convergence from free-stream conditions to a realistic state. This is achieved by assigning to each cell the maximum allowable time step for a given CFL number (pseudo time marching). Global time stepping is then turned on before unsteady data is sampled.

In order to evaluate the total drag, the momentum deficit method is used by evaluating the velocity deficit in the wake of the landing gear. More details can be found in Rae and Pope[16]. Figure 6 shows the average velocity deficit right behind the second gear configuration.

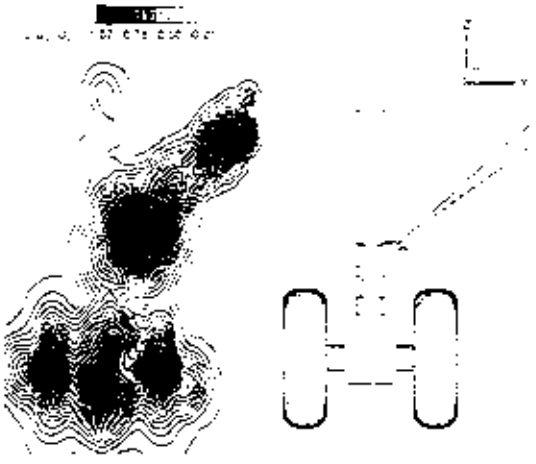

Figure 6- Average velocity deficit in the wake of the second landing gear configuration (LDG2)

In the second gear case, there is a good qualitative agreement with experimental results published by Stoker[7] in the high-fidelity landing gear configuration. Figure 7 shows the drag forces computed by integrating the pressure on the gear surface (pressure drag) and using Pope's wake deficit approach (labeled total drag). Results are shown for both gear configurations during approximately 7 milliseconds of simulated flow time, giving enough time for the fluid to cover three times the gear total length. The force coefficients (drag, lateral and vertical force) are the computed forces divided by the landing gear surface area and the dynamic pressure.

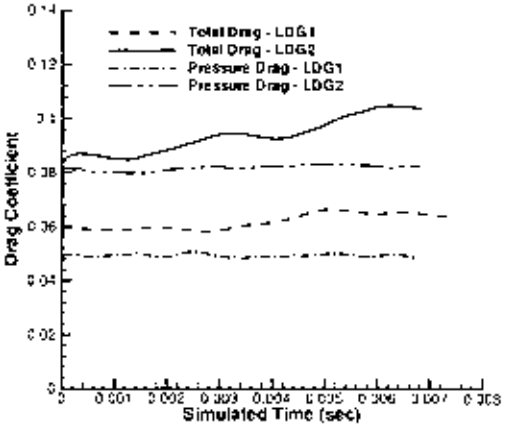

Figure 7- Time-history of drag force coefficients for landing gear configurations 1 (LDG1) and 2 (LDG2) using pressure and wake methods

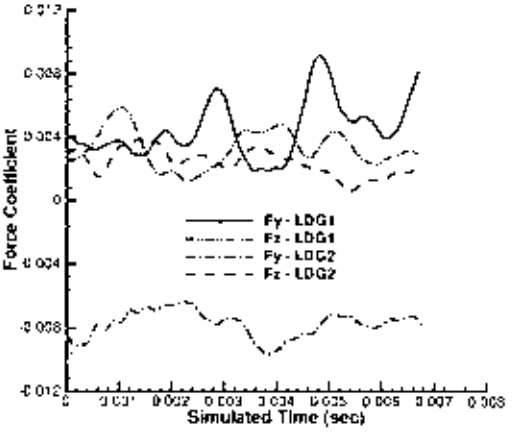

Figure 8- Time-history of lateral (Fy) and vertical (Fz) force coefficients for landing gear configurations 1 (LDG1) and 2 (LDG2)

The increase in overall drag due to the introduction of the lateral support struts is large since these components are not aerodynamically profiled and are comparable to flat plates facing the incoming fluid flow. Figure 8 illustrates the lateral forces stemming from the presence of these two struts.

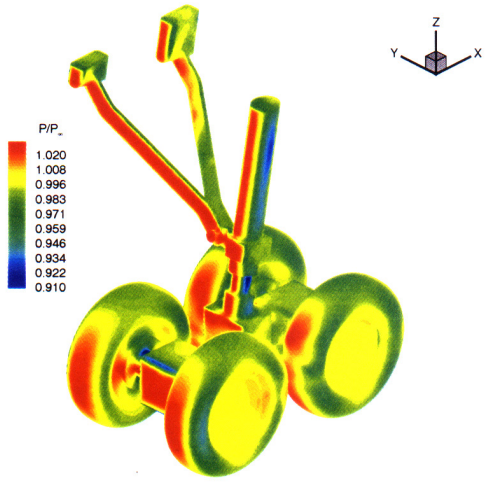

Figure 9- Instantaneous pressure distribution for the second landing gear configuration (LDG2)

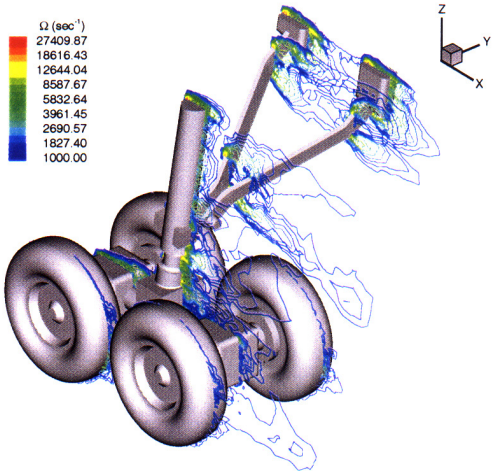

Figure 10- Instantaneous vorticity filaments for the second landing gear configuration (LDG2)

One expects the far-field sound pressure level to reflect this unsteady loading in both its intensity and directivity. Figure 9, which is a display of the instantaneous distribution of pressure on the landing gear surface in its second configuration, shows the pressure on these support struts, as well as on the wheels.

Figure 10 shows a 3D representation of some vortex filaments shedding off various gear components, and highlight the impact of the upstream elements' wake onto gear elements at downstream locations.

The effect of these vortices is not completely captured by the FW-H surface which lies on the landing gear itself. However the permeable FW-H surface does account for all the effects induced by these filaments until they cross its boundaries.

FAR-FIELD NOISE PREDICTION

Only recently has the FW-H equation been used on a permeable surface. di Francescantonio[17] was able to show that simply integrating the surface source terms on a porous FW-H surface does account for the quadrupole sources enclosed within the surface. The FW-H equation is written in the standard differential form including all quadrupole, dipole and monopole source terms as

$$\Box^2 p'(\mathbf{x},t) = \frac{\partial^2}{\partial x_i \partial x_j}\left[T_{ij} H(f)\right] - \frac{\partial}{\partial x_i}\left[L_i \delta(f)\right] + \frac{\partial}{\partial t}\left[(\rho_o U_n)\delta(f)\right] \quad (1)$$

where L_i and U_n are defined as

$$U_n = U_i \hat{n}_i \quad U_i = \left(1 - \frac{\rho}{\rho_o}\right) v_i + \frac{\rho u_i}{\rho_o}$$

$$L_i = P_{ij}\hat{n}_j + \rho u_i (u_n - v_n) \quad (2)$$

and T_{ij} is the Lighthill stress tensor. $\Box^2$ is the wave operator defined as:

$$1/c^2\,\partial^2/\partial t^2 - \nabla^2 .$$

In equation 2, ρ is the total density, ρu_i is the momentum in the i direction, v_i is the velocity of the integration surface f = 0, and P_{ij} is the compressive stress tensor. The subscript n indicates the projection of a vector quantity in the surface normal direction. Using the solution to the above equation given in Brentner and Farassat[18] and neglecting the quadrupole terms, the pressure fluctuation at a given observer location **x** and time t is (equation 3 below)

$$4\pi p'(\mathbf{x},t) = \int_{f=0}\left\{\left[\frac{\rho_0 \dot{U}_n}{r(1-M_r)^2}\right] + \left[\frac{\rho_0 U_n c(M_r - M^2)}{r^2(1-M_r)^3}\right]\right\}_{ret} dS + \int_{f=0}\left\{\frac{1}{c}\left[\frac{\dot{L}_r}{r(1-M_r)^2}\right] + \left[\frac{L_r - L_M}{r^2(1-M_r)^2}\right] + \left[\frac{L_r(M_r - M^2)}{r^2(1-M_r)^3}\right]\right\}_{ret} dS$$

FW-H code validation

In the absence (at the moment) of experimental acoustic data to compare to, an already-proven method was implemented: the use of the CFD results to validate the FW-H sound predictions. As was done by the authors in a previous test case[8], the pressure fluctuations computed by the flow solver PUMA at an observer in the near field were compared with the predictions given by the FW-H post-processing utility. Although the near-field pressure fluctuations are large, and likely contain a great amount of hydrodynamic oscillations, the derivation of the FW-H equation is such that all pressure perturbations (acoustic and hydrodynamic) should be recovered. Examples in the near field are given by Farassat and Brentner[19] in the case of high-speed impulsive noise at rotor blade tip Mach number close to 0.9. It is assumed that at a Mach number of 0.2, the quadrupole terms do not contribute significantly to the far-field noise. The solution to the quadrupole term of the FW-H equation is:

$$4\pi\, p'_Q(\mathbf{x},t) = \frac{\partial^2}{\partial x_i \partial x_j}\int_{-\infty}^{t}\int_{f>0}\frac{T_{ij}}{r}\, c\, d\Omega\, d\tau \quad (4)$$

The volume integration, if performed, must be carried out over a large volume and represents a large computational task. The far field approximation of equation 4 reduces to:

$$4\pi\, p'_Q(\mathbf{x},t) = \frac{1}{c}\frac{\partial^2}{\partial t^2}\int_{-\infty}^{t}\int_{f>0}\frac{T_{rr}}{r}\, d\Omega\, d\tau \quad (5)$$

However, there is in the present case an interest in capturing quadrupole effects in the near field, so that an exact result to the FW-H is needed instead of the far field approximation. Farassat and Brentner[20] decomposed the quadrupole noise term into three components varying with $1/r$, $1/r^2$ and $1/r^3$ respectively:

$$\begin{aligned} 4\pi p'_Q(\mathbf{x},t) = & \frac{1}{c}\frac{\partial^2}{\partial t^2}\int_{-\infty}^{t}\int_{f>0}\frac{T_{rr}}{r}\, d\Omega\, d\tau \\ & + \frac{\partial}{\partial t}\int_{-\infty}^{t}\int_{f>0}\frac{3T_{rr} - T_{ii}}{r^2}\, d\Omega\, d\tau \\ & + c\int_{-\infty}^{t}\int_{f>0}\frac{3T_{rr} - T_{ii}}{r^3}\, d\Omega\, d\tau \quad (6) \end{aligned}$$

There is a possibility that the second and third terms may contribute in a significant way to the near field pressure variations. This implies that in order to validate the FW-H predictions against the CFD results one may have to account for some of these nonlinear effects in addition to loading noise in the near field since the observer is in a highly perturbed propagating medium. In the current derivation of the FW-H equation, the quadrupole term is not computed (to reduce computing time and to limit storage requirements). However the porous FW-H surface shown in a previous figure has the ability to recover all nonlinear effects occurring within its own boundaries. Figure 11 is an illustration of the instantaneous pressure distribution on the permeable FW-H integration surface.

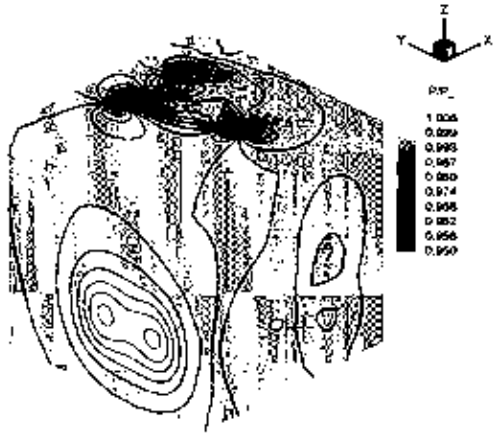

Figure 11- Instantaneous pressure distribution on permeable FW-H surface for second landing gear configuration (LDG2)

Observers were placed just above the landing gear main leg (x = 2.68 cm, y = 0 cm and z = 17 cm for observer whose pressure is depicted in Figure 12), where the porous FW-H mesh is more refined, so that the FW-H predictions can take place using both the solid and the porous FW-H surfaces. An example of

comparisons with the PUMA results at one of these near-field observer locations is shown in Figure 12. This shows good agreement between the porous FW-H predictions and the solver computation, even though the solid FW-H surface misses by more than 50% some of the pressure fluctuations.

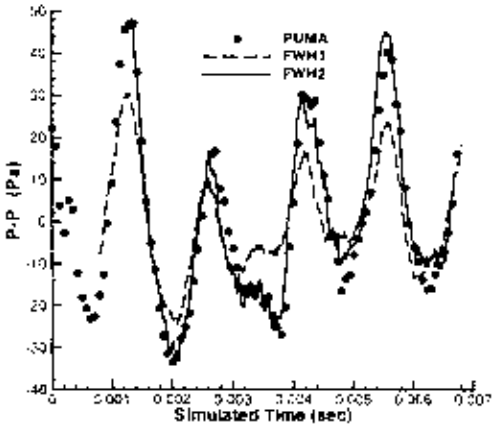

Figure 12- Comparison of FW-H predictions from integration surfaces 1 and 2 vs. PUMA results in the near-field

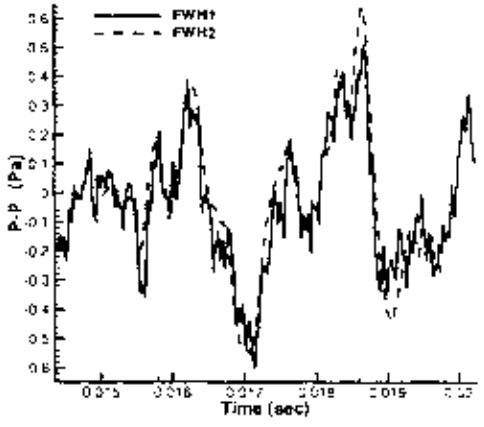

Figure 13- Comparison of FW-H predictions from integration surfaces 1 and 2 in the far-field

This demonstrates the ability of the second FW-H surface to predict the entire pressure oscillations, either of acoustic or hydrodynamic nature. It tends to suggest that quadrupole effects may represent a significant contribution to the overall near-field sound level even at moderate Mach numbers. Unless a volume integration is performed over the entire CFD domain, the entire pressure perturbation cannot be exactly reproduced where nonlinear effects are important and where vortices flow across the permeable FW-H surface.

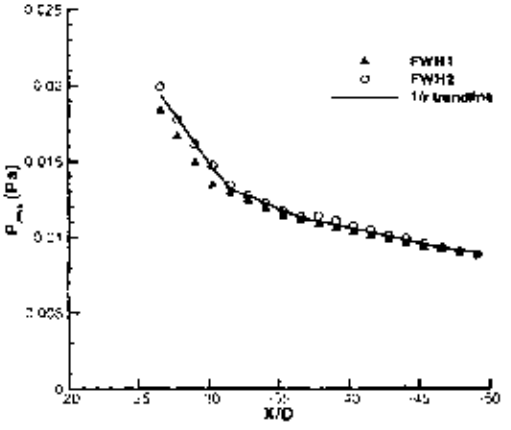

Figure 14- RMS pressure signal predictions from integration surfaces 1 and 2 and trend lines

As expected, the agreement between the predictions from the two FW-H surfaces improves in the far-field. Figure 13 shows the pressure time history at 40 radii from the landing gear at a 50 degree angle with respect to the downstream axis.

The field produced by the coarser FW-H surface off the landing gear does not reflect the same high-frequency fluctuations given by the predictions coming from data collected on the gear itself. In view of experimental results described earlier, it was decided to use the solid FW-H surface to investigate the far-field noise directivity, where high-frequency signals are thought to be significant. Figure 14 below illustrates the decrease of the RMS pressure signal as one moves away from the landing gear along the downstream axis.

Calculations were made at 20 observers from 25 wheel diameters down to 50 wheel diameters in the wake of the landing gear. Both FW-H surface data were used and compared with a trend line assuming a signal decaying with 1/r.

As observed previously, the agreement between the two surface predictions improves with increasing distance from the landing gear. As one moves further away from the landing gear, it is seen by the observer as an acoustic compact source, and the signal intensity should decrease with the inverse of the distance from the source.

Sound directivity patterns

The sound directivity in the medium- and far-field requires the use of a parallel version of the FW-H post-processing program[8,21]. For each radii away from the landing gear, 72 observer locations are defined, so that a resolution of 5 degree angle is obtained. A total of 648 observer points were defined, and are illustrated in Figure 15, which shows the relative scale with respect to the landing gear. For both gear configurations, all three orientation planes were studied and the results are reported in Figures 16a to 16f, Figures 17a to 17f and Figures 18a to 18f for the first and second gear configurations from a streamwise, spanwise and vertical perpective respectively. Polar directivity plots at radial locations of 10, 15 and 20 radii from the gear are plotted separately from the locations further away (30 to 50 radii from the gear) for scaling issues. Sound Pressure Level (SPL) contours with a reference pressure of $6x10^{-6}$ Pa are also presented for radial locations varying from 25 to 50 radii from the landing gear. The scale for equivalent configurations is unchanged in order to allow for qualitative comparisons with respect to both directivity and intensity of the sound pressure signal. In Figures 16 to 18, the landing gear is not to scale, and is meant to illustrate which orientation axis is shown.

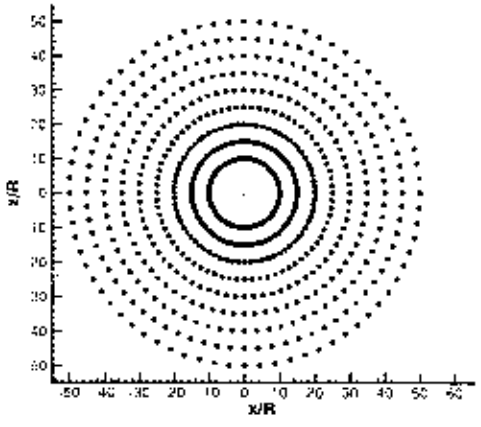

The drag augmentation is reflected in the sound directivity patterns of both configurations. The intensity of the RMS pressure is greatly increased along the streamwise direction for the second gear case (LDG2). This is due to the two support struts on the aerodynamic profile of the landing gear. Regarding the lateral noise, the two struts seem to interfere with the build-up of sound, so that the signal in the spanwise direction is less than that in the clean configuration, where varying lateral forces on the gear leg create pressure levels in the far-field comparable to those along the streamwise direction. In both cases, the near-field pressure perturbations are dominated by the fluctuations in drag. Very little near-field noise is generated in the spanwise or vertical directions. The overall pressure field looks much more disturbed in the second gear configuration, illustrating the complex three-dimensionality of the noise-generating flow pattern.

CONCLUSION

The flow field around two landing gear configurations of increasing complexity has been assessed. The wake defect observed behind the landing gear is very similar to that experimentally measured on comparable configurations. A parallel version of the Ffowcs Williams – Hawkings equation has been implemented using inexpensive Beowulf clusters to extract near- and far-field sound information. Both solid and permeable FW-H integration surfaces have been used. Excellent agreement has been obtained in the near field between the porous FW-H surface predictions and the CFD solver results where hydrodynamic fluctuations are expected to dominate and are of greater magnitudes than those typical of acoustic signals. More work is needed in order to show that the discrepancy observed between the solid and porous FW-H surfaces in the near-field is linked to short-range quadrupole-like effects even though the problem that was dealt with in the present case is a relatively low Mach number flow for this kind of effects to be significant.

The comparison of acoustic predictions produced by the two FW-H surfaces improves as the observer location is moved further away in the far field. The increase in drag stemming from the lateral struts is reflected in the noise level and directivity. There is a significant increase in sound intensity in the streamwise direction, whereas the disturbance caused by these gear elements seems to interfere with the vortex shedding off the gear leg and the resulting lateral sound radiation.

FUTURE WORK

A parallel investigation on separated flow around a cone[22] shows that the implementation of a Large Eddy Simulation (LES) method using a Smagorinsky sub-grid scale model significantly improves PUMA's accuracy to simulate both mean and turbulent quantities

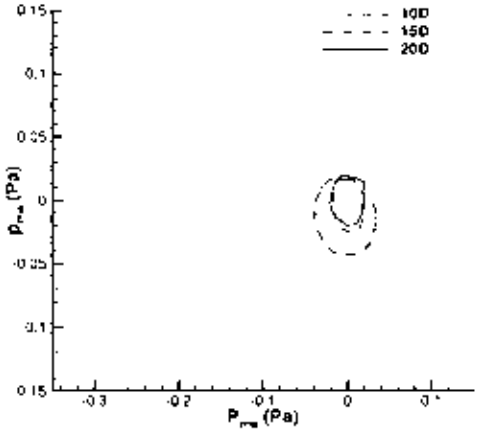

Figure 16a

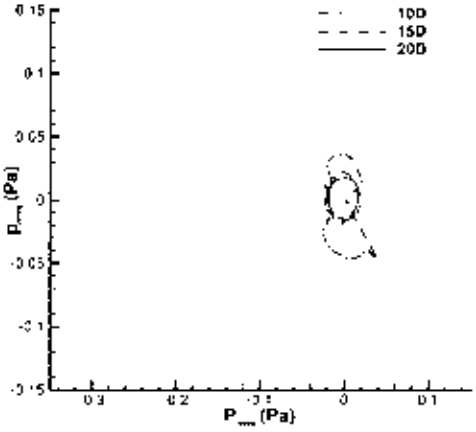

Figure 16d

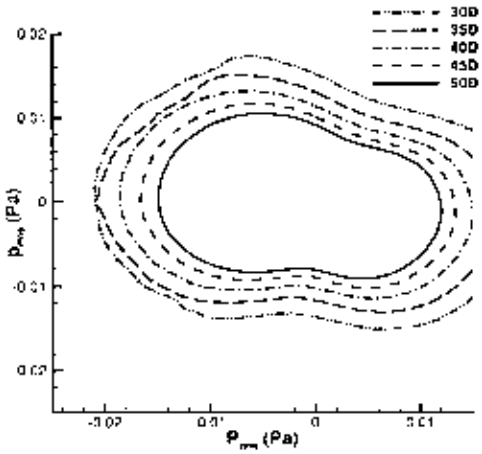

Figure 16b

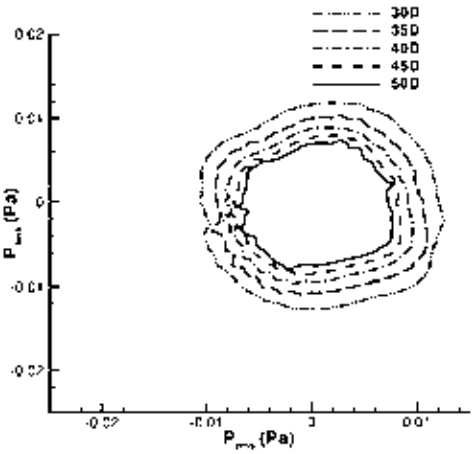

Figure 16e

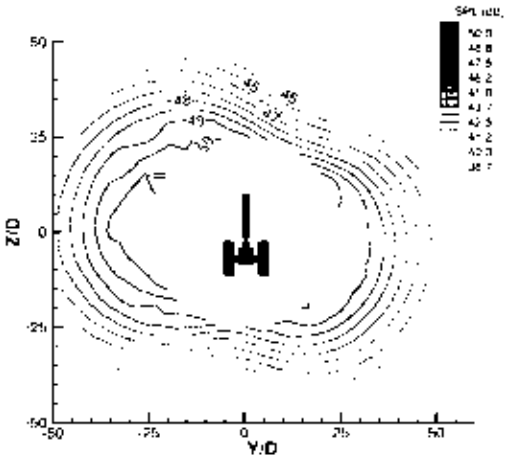

Figure 16c: (a) Medium-field RMS pressure, (b) far-field RMS pressure, (c) SPL contour for LDG1 from streamwise perspective

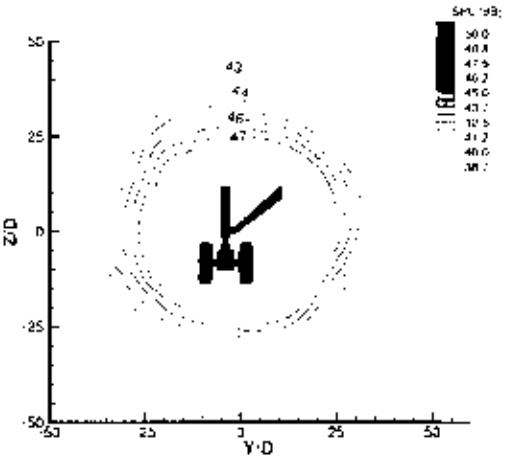

Figure 16f: (d) Medium-field RMS pressure, (e) far-field RMS pressure, (f) SPL contour for LDG2 from streamwise perspective

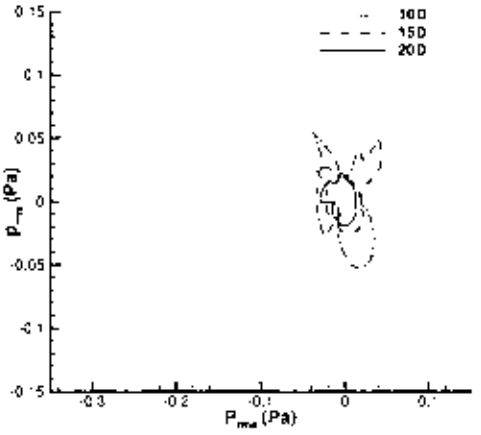

Figure 17a

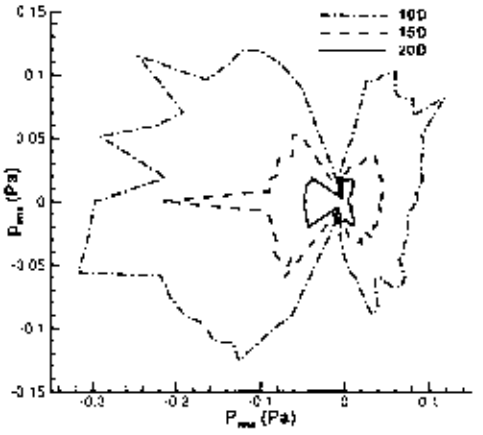

Figure 17d

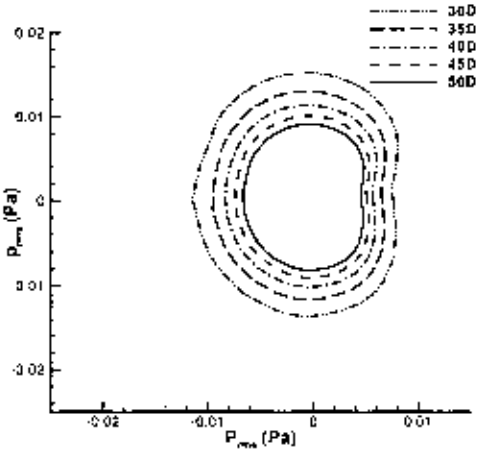

Figure 17b

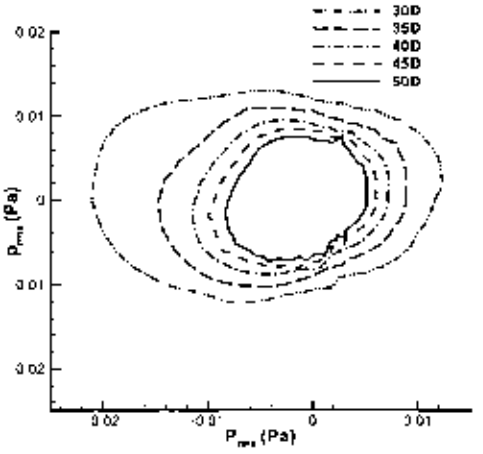

Figure 17e

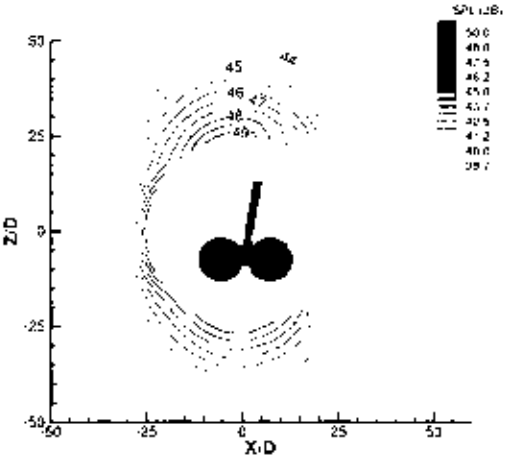

Figure 17c: (a) Medium-field RMS pressure, (b) far-field RMS pressure, (c) SPL contour for LDG1 from sideways perspective

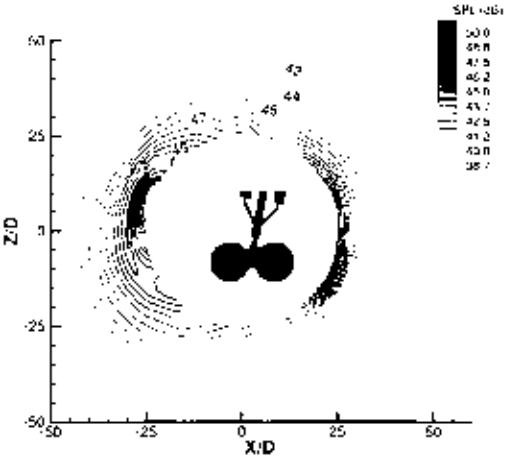

Figure 17f: (d) Medium-field RMS pressure, (e) far-field RMS pressure, (f) SPL contour for LDG2 from sideways perspective

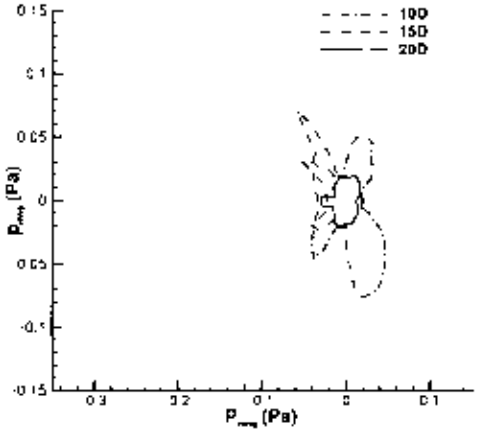

Figure 18a

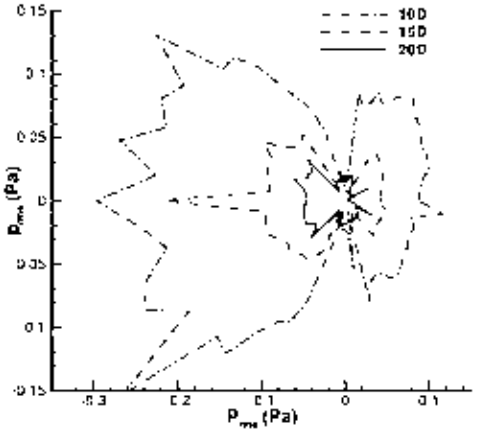

Figure 18d

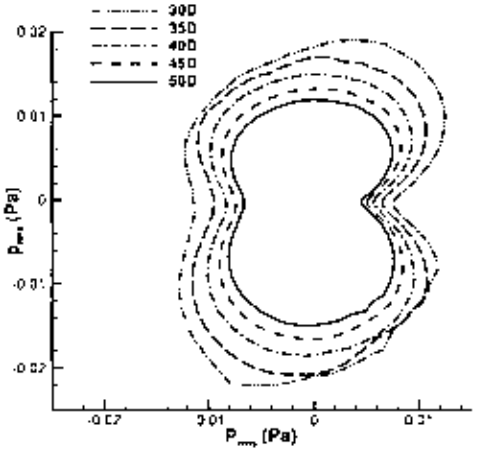

Figure 18b

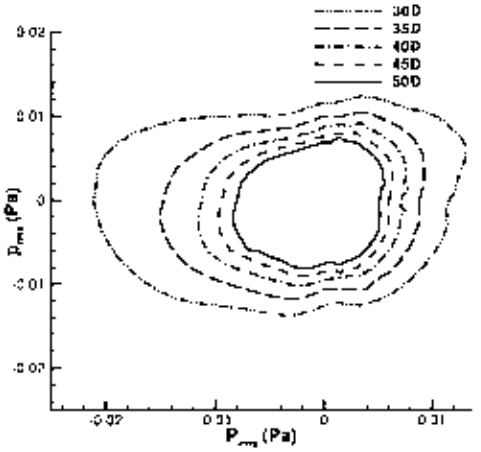

Figure 18e

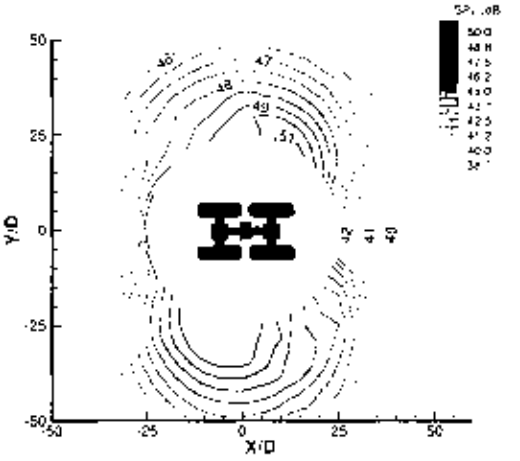

Figure 18c: (a) Medium-field RMS pressure, (b) far-field RMS pressure, (c) SPL contour for LDG1 seen from above

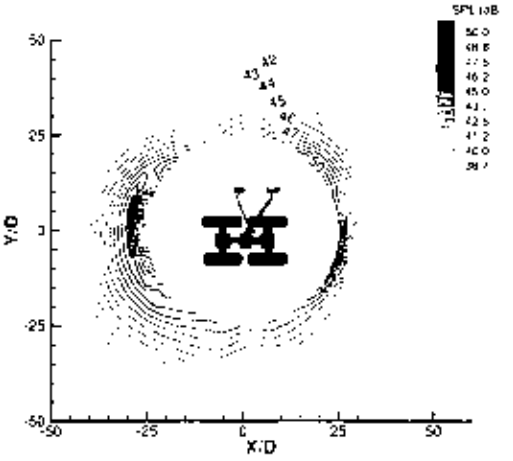

Figure 18f: (d) Medium-field RMS pressure, (e) far-field RMS pressure, (f) SPL contour for LDG2 seen from above

in the wake of a cone base flow. LES has already been used extensively to compute sound sources[23,24], but some recent work related to two-time statistics of LES data, would indicate that LES fields are too coherent if the eddy viscosity model does not include any random backscatter[25]. One way to circumvent this may be the use of a dynamic LES, which is more likely to yield enough backscattering to decorrelate the fluid motion at large scales. An example of the use of a dynamic subgrid scale model combined with a Ffowcs Williams – Hawkings solver is given by Morris et al[26] in an attempt to simulate the jet noise for circular nozzles.

The experience gained between both cases shows that more CAD and meshing work can be done in order to maximize the allowable time-step and simulate as many shedding cycles as possible: this helped double the time step. It is worth mentioning though that the existing amount of data for both gear configurations already puts a strain on the available capacity in terms of storage requirements: about 40 Gigabytes of data have been collected for the two calculations described in this study.

Other configurations should be tested in order to investigate the impact of various gear elements on the flow field and the resulting far-field sound level: the original CAD file contained a side door which was removed for simplification purpose. Another test case also is to implement an inviscid boundary condition on top of the gear leg to simulate the installation effects under a wing or fuselage.

REFERENCES

[1]Singer, B. A., Brentner, K. S., Lockard, D. P. and Lilley, G. M., "Simulation of Acoustic Scattering from a Trailing Edge", Paper 1999-0231, 37th Aerospace Sciences Meeting and Exhibit", Reno, NV, 1999.

[2]Singer, B. A., Lockard, D. P., Brentner, K. S., Khorrami, M. R., Berkman, M. E. and Choudhari, M., "Computational Aeroacoustic Analysis of Slat Trailing-Edge Flow", Paper 1999-1802, 5th AIAA/CEAS Aeroacoustics Conference, Greater Seattle, WA, 1999.

[3]Özyörük, Y. and Long, L. N., "A New Efficient Algorithm for Computational Aeroacoustics on Parallel Processors", Journal of Computational Physics, Vol. 125, pp. 135-149.

[4]Heller, H. H. and Dobrzynski, W. M., "Sound Radiation From Aircraft Wheel-Well/Landing-Gear Configurations", *J Aircraft*, vol. 14, no. 8, Aug. 1977, pp.768-774.

[5]Dobrzynski, W. M. and Buchholz, H., "Full-Scale Noise Testing on Airbus Landing Gears in the German Dutch Wind Tunnel", AIAA-97-1597.

[6]Dobrzynski, W., Chow, L. C., Guion P. and Shiells, D., "A European Study On Landing Gear Airframe Noise Sources", Paper 2000-1971, 6th AIAA/CEAS Aeroacoustics Conference and Exhibit, Lahaina, HI, 2000.

[7]Stoker, R. W. and Sen, R., "An Experimental Investigation of Airframe Noise Using a Model-Scale Boing 777", Paper 2001-0987, 39th Aerospace Sciences Meeting and Exhibit", Reno, NV, 2001.

[8]Long, L. N., Souliez, F. and Sharma, A., "Aerodynamic Noise Prediction Using Parallel Methods on Unstructured Grids", Paper 2001-2196, 7th AIAA/CEAS Aeroacoustics Conference, Maastricht, The Netherlands, 2001.

[9]Modi, A. and Long, L. N., "Unsteady Separated Flow Simulations using a Cluster of Workstations", Paper 2000-0272, 38th Aerospace Sciences Meeting and Exhibit", Reno, NV, 2000.

[10]Sharma, A. and Long, L. N., "Airwake Simulations on LPD17 Ship", Paper 2001-2589, 31st AIAA Fluid Dynamics Conference and Exhibit, Anaheim, CA, 2001.

[11]Strelets, M., "Detached Eddy Simulation of Massively Separated Flows", Paper 2001-0879, 39th Aerospace Sciences Meeting and Exhibit", Reno, NV, 2001.

[12]http://www.pointwise.com/

[13]Duff, I. S., Erisman, A. M. and Reid, J. K., Direct Methods for Sparse Matrices, Oxford University Press, 1986.

[14]http://cocoa.ihpca.psu.edu/

[15]http://cocoa2.ihpca.psu.edu/

[16]Rae, W. H. and Pope, A., "Low-Speed Wind Tunnel Testing", second edition, Wiley-Interscience, 1984.

[17]di Francescantonio, P., "A New Boundary Integral Formulation for the Prediction of Sound Radiation", *Journal of Sound and Vibration* (1997) 202(4), pp. 491-509.

[18]Brentner, K. S., and Farassat, F., "An Analytical Comparison of the Acoustic Analogy and Kirchhoff Formulation for Moving Surfaces" *AIAA Journal*, Vol. 36, No .8, Aug. 1998, pp. 1379-1386.

[19]Farassat, F. and Brentner, K. S., "Supersonic Quadrupole Noise Theory for High-Speed Helicopter Rotors", *Journal of Sound and Vibration* (1998) 218(3), pp. 481-500.

[20]Farassat, F. and Brentner, K. S., "The Uses and Abuses of the Acoustic Analogy in Helicopter Rotor Noise Prediction", *Journal of the American Helicopter Society* (1988) 33, pp. 29-36.

[21]Long, L. N. and Brentner, K. S., "Self-Scheduling Parallel Methods for Multiple Serial Codes with Application to WOPWOP", Paper 2000-0346, 38th Aerospace Sciences Meeting and Exhibit", Reno, NV, 2000.

[22]Souliez, F. J., Parallel Methods for Computing Unsteady Separated Flows Around Complex Geometries, PhD thesis, Penn State University.
[23]Piomelli, U., "Large-Eddy Simulation: Achievements and Challenges", Progress in Aerospace Sciences 35 (1999), pp. 335-362.
[24]Seror, C., Sagaut, P., Bailly, C. and Juve, D., "On the Radiated Noise Computed by Large-Eddy Simulation", Phys. Fluids 13 (2001), pp. 476-487.
[25]He, G., Rubinstein, R. and Wang, L. P., "Effects of Eddy Viscosity on Time Correlations in Large Eddy Simulation", ICASE Report No. 2001-10.
[26]Morris, P. J., Scheidegger, T. E. and Long, L. N., "Jet Noise Simulations for Circular Nozzles", Paper 2000-2080, 6th AIAA/CEAS Aeroacoustics Conference and Exhibit, Lahaina, HI, 2000.